Journal of Inflammation Research

Dovepress
Taylor & Francis Group

Open Access Full Text Article

ORIGINAL RESEARCH

Retinoic Acid-Loaded Cartilage Organoids Attenuate Chondrocyte Senescence in Osteoarthritis

Liang Xi*, Yongfeng Chen*, Zhuojing Luo, Dawei Zhang

Department of Orthopaedics, Xijing Hospital, Fourth Military Medical University, Xi'an, People's Republic of China

*These authors contributed equally to this work

Correspondence: Zhuojing Luo; Dawei Zhang, Email lzjammu@163.com; xijingzdw@163.com

Background: Osteoarthritis (OA) is a debilitating degenerative joint disease characterized by chondrocyte senescence and cartilage degradation. Despite extensive research, effective therapeutic strategies targeting the underlying mechanisms of chondrocyte senescence remain limited.

Methods: We employed an integrated multi-omics approach combining weighted gene co-expression network analysis (WGCNA) and machine learning algorithms with the SenMayo gene set to identify key senescence-associated genes in OA. Single-cell RNA sequencing was used to characterize distinct chondrocyte subpopulations. Computational screening, molecular docking, and dynamics simulations identified potential therapeutic compounds. We engineered a triphasic gelatin methacryloyl/hyaluronic acid methacryloyl (GelMA/HAMA) cartilage organoid system for controlled delivery of retinoic acid (RA) and evaluated its efficacy in vitro and in a rat destabilization of the medial meniscus (DMM) model of OA.

Results: Our bioinformatic analysis identified *ANGPT1, MMP1, EGF*, and *IGF1* as critical senescence-associated genes in OA, forming the basis for a robust clinical prediction model (area under the curve [AUC] = 0.931). Single-cell analysis revealed dysregulated TGF-β1 signaling as central to senescence-mediated cartilage degeneration. In vitro, RA attenuated chondrocyte senescence by activating the TGFβ/Smad pathway, reducing apoptotic markers, and restoring extracellular matrix components. The biomimetic cartilage organoid system facilitated spatiotemporally controlled release of RA within the joint environment. When implanted in the rat OA model, these RA-loaded organoids significantly reduced cartilage degeneration as evidenced by improved Osteoarthritis Research Society International (OARSI) scores, enhanced tissue architecture, and increased cartilage thickness.

Conclusion: Our findings establish RA delivered via biomimetic cartilage organoids as a promising therapeutic strategy that addresses the cellular mechanisms underlying OA progression. This approach may represent a paradigm shift from symptom management to disease modification by targeting chondrocyte senescence and promoting cartilage regeneration, offering new avenues for developing effective treatments for OA.

Keywords: senescence, TGFβ, retinoic acid, cartilage organoid, osteoarthritis

Introduction

Osteoarthritis (OA) is a widespread degenerative joint disorder that markedly reduces quality of life and imposes a significant socioeconomic burden.[1] Although current therapies—ranging from pain management and physical therapy to joint replacement—primarily address symptoms, they rarely alter the disease's progression.[2,3] This limitation largely reflects an incomplete understanding of the molecular drivers underlying OA. Chondrocytes and their surrounding extracellular matrix (ECM)—predominantly composed of collagen II, hyaluronic acid, and proteoglycans—are essential for maintaining cartilage integrity.[4,5] Consequently, dissecting the molecular alterations in chondrocytes during OA progression is critical for developing therapies that not only relieve symptoms but also modify disease outcomes.

Recent studies have underscored the pivotal role of chondrocyte senescence in OA.[6] Senescent chondrocytes exhibit reduced proliferative capacity and cell cycle arrest while releasing a senescence-associated secretory phenotype (SASP) rich in pro-inflammatory cytokines, chemokines, and matrix-degrading enzymes.[7,8] The accumulation of these cells is closely

Received: 9 June 2025
Accepted: 27 October 2025
Published: 4 November 2025

linked to increased inflammation and cartilage degradation, largely mediated by pathways such as nuclear factor-kappa B (NF-κB).[9] Thus, interventions aimed at suppressing SASP secretion, modulating inflammatory signaling, or restoring a balanced cellular environment may provide novel strategies to delay OA progression.

In recent years, the rapid development of multi-omics technologies has provided unprecedented insights into the molecular underpinnings of OA.[10,11] By integrating bulk transcriptomics with single-cell RNA sequencing (scRNA-seq), researchers can now dissect cell type–specific gene expression profiles within the joint.[12,13] This integrative approach has revealed distinct regulatory patterns of SASP factors among various chondrocyte subpopulations, enabling the precise identification of key SASP components and their regulatory networks.[14] Such detailed molecular mapping is instrumental in uncovering novel therapeutic targets for mitigating chondrocyte senescence and promoting cartilage repair.

Current therapies primarily address symptoms and fail to reverse or halt cartilage degeneration at the cellular level. Emerging tissue-engineered cartilage organoids offer a promising avenue to overcome these limitations by recapitulating native tissue architecture and function.[15] These three-dimensional constructs derived from biomimetic hydrogels, such as gelatin methacryloyl (GelMA) and hyaluronic acid derivatives, can encapsulate chondrocytes or progenitor cells within a supportive microenvironment that promotes cell proliferation, phenotype maintenance, and extracellular matrix production. Importantly, cartilage organoids can be engineered to deliver bioactive molecules, which has been shown to attenuate chondrocyte senescence by modulating signaling pathways involved in cellular aging and inflammation.[16,17] Thus, cartilage organoids represent a versatile platform for developing disease-modifying treatments targeting the cellular and molecular mechanisms underlying OA progression.

In this study, we employed an integrated omics approach to investigate the relationship between chondrocyte senescence and OA pathogenesis. We hypothesized that retinoic acid (RA) could reverse chondrocyte senescence by modulating the transforming growth factor-beta/Smad (TGFβ/Smad) signaling pathway, thereby restoring cartilage homeostasis in osteoarthritis. By applying the specialized SenMayo gene set together with weighted gene co-expression network analysis and machine learning algorithms, we identified four critical senescence-associated genes in OA chondrocytes.[18] ScRNA-seq analysis further enabled precise characterization of senescent chondrocyte subpopulations and revealed the pivotal role of dysregulated TGF-β1 signaling in driving senescence-mediated cartilage degeneration. Based on this hypothesis, through computational screening, molecular docking, and dynamics simulations, we identified RA as a promising therapeutic agent targeting these senescence mechanisms. In vitro experiments confirmed RA's capacity to attenuate chondrocyte senescence via activation of the TGFβ/Smad pathway, while our in vivo studies demonstrated that RA delivered through a novel triphasic GelMA/ hyaluronic acid methacryloyl (HAMA) cartilage organoid system enhanced ECM synthesis, reduced catabolic activity, and improved cartilage integrity in a rat OA model. The workflow of this comprehensive investigation is illustrated in Figure 1.

Materials and Methods

Microarray Datasets

We extracted bulk transcriptome data from the cartilage and synovium tissues of 29 non-arthritic individuals and 29 osteoarthritic joints from three microarray datasets (GSE12021, GSE55457, and GSE55235) hosted in the Gene Expression Omnibus database. All the datasets were sequenced using the GPL96 platform. Additionally, scRNA-seq data were obtained from three non-arthritic and four osteoarthritic patients (GSE169454), focusing on articular cartilage cells.[19]

Data Processing and Differential Analysis

All bioinformatic statistical analyses and visualizations were performed using R version 4.2.1. Batch effects were mitigated after matrix normalization via the "combat" function of the "sva" package. Differentially expressed genes (DEGs) were identified using the "limma" package, adhering to a threshold of $|\log_2(\text{fold-change})| > 0.575$, with an adjusted P-value < 0.05. Heatmaps were generated using the "pheatmap" package, and gene function enrichment was analyzed using online bioinformatics resources and the GeneMANIA website (https://genemania.org/).

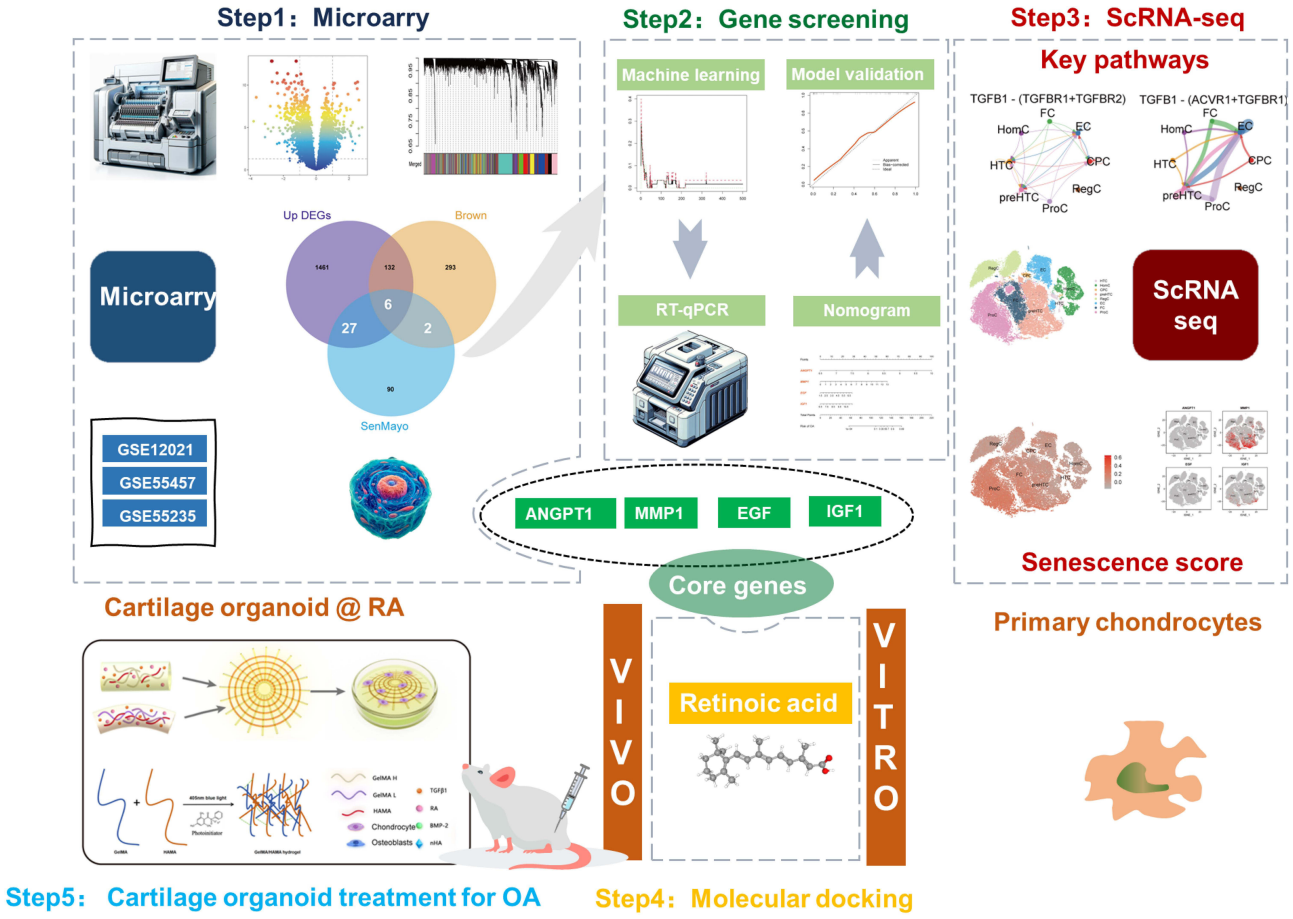

Figure 1 Flow-diagram for the study.
Abbreviations: DEGs, differentially expressed genes; WGCNA, weighted gene coexpression network analysis; RA, Retinoic Acid.

Weighted Gene Co-Expression Network Analysis (WGCNA)

WGCNA was conducted using the "WGCNA" package to identify gene modules with similar expression patterns. After filtering for genes with a variance greater than 25%, the soft-thresholding power was set to 6, as determined using the pickSoftThreshold function. Modules were formed using average linkage hierarchical clustering, based on the topological overlap matrix (TOM) dissimilarity measure, and the correlation between each module and the presence of OA was evaluated.

Identification of Key Aging-Associated Genes

Using the SenMayo gene set, which identifies senescence-associated pathways across tissues, we intersected modules highly correlated with OA with upregulated DEGs.[18] Key genes were further refined using machine learning techniques via the "randomForest" package and were subsequently visualized and analyzed using the "ggpubr" package.[20]

Establishment and Validation of a Nomogram

A predictive model was constructed based on the $\log_2|\text{FPKM}|$ values for each gene. Comprehensive analysis of hub genes and model construction were performed using the "rms" package, creating a nomogram based on these risk genes. The reliability of the model was internally validated using the "caret" package. This analysis included calibration, clinical decision analysis, and the construction of receiver operating characteristic (ROC) curves.

scRNA-Seq Data Processing

scRNA-seq data were processed using the Seurat software package. Cells with expressed gene counts outside the range of 300–6000, mitochondrial gene counts exceeding 20%, or RNA counts above the 98th percentile were excluded. Additionally, more than three cells were required to express the genes and the red blood cell gene expression proportion was required to be less than 0.05. Highly variable genes were identified using the "FindVariableGenes" function, followed by principal component analysis (PCA) for data reduction. Data visualization at the single-cell level was performed using t-distributed stochastic neighbor embedding (t-SNE). The "Harmony" package was used to integrate the data across different tissue samples to effectively mitigate batch effects. Gene expression differences were identified using the "FindAllMarkers" function, applying a threshold of $|\log_2(\text{fold-change})| > 0.8$ and an adjusted p-value < 0.05.

Single-cell distributions were visualized using the "DimPlot" function, while gene expression patterns were depicted through the "FeaturePlot" function. Cell subgroups were annotated based on classifications used in previous studies.[19] The "plot1cell" package was used for the dot plot visualization of grouped data. Cell developmental trajectories were analyzed using the "Monocle2" package, and intercellular communication networks were constructed using "CellChat." Cellular aging scores were calculated using the "AddModuleScore" function based on the SenMayo gene set to evaluate aging-related differences across cells.

Molecular Modeling Analysis

We utilized the DSigDB database to predict the interactions between Food and Drug Administration–approved compounds and key aging-related genes, with a significance threshold of $P < 0.05$. The two-dimensional structures of the compounds were retrieved from the PubChem database, and protein structures were obtained from the RCSB Protein Data Bank. Molecular interactions between small molecules and target proteins were modeled using AutoDock 4 software, and visualization was performed using PyMol software.[21]

Molecular Dynamics Simulation

A 100 ns MD simulation was conducted using GROMACS 2022 for the protein–ligand complex. The protein was parameterized using the CHARMM36 force field, while the ligand topology was generated with GAFF2 parameters.[22] The complex was placed in a cubic box with periodic boundary conditions and solvated using the TIP3P water model, ensuring a minimum buffer distance of 1.2 nm between the solute and the box edges. Electrostatic interactions were computed using the Particle Mesh Ewald method, and the Verlet algorithm was employed for updating the neighbor lists. Following energy minimization, the system underwent equilibration under the NVT and NPT ensembles, each for 100,000 steps with a coupling constant of 0.1 ps over a 100 ps duration. Both van der Waals and Coulomb interactions were calculated with a 1.0 nm cutoff. Subsequently, a production MD simulation was performed for 100 ns under constant temperature (310 K) and pressure (1 bar).

Animal Preparation and Surgery

All animal procedures were approved by the Animal Research Ethics Committee of the Fourth Military Medical University (Xi' an, China). Adult male Sprague-Dawley (SD) rats (6 weeks old, n = 9, weighing 200–250 g) were obtained from the Laboratory Animal Center of the Fourth Military Medical University. Animals were housed in groups of three per cage under controlled environmental conditions (temperature and 12-h light/dark cycle) at Xijing Hospital, Xi'an, China, with *ad libitum* access to sterile food and water.

OA was induced by the surgical destabilization of the medial meniscus (DMM). The rats were anesthetized using a ketamine-xylazine cocktail. A 3-mm longitudinal incision was made to expose the area from the distal femur to the proximal tibia, and the medial meniscotibial ligament (MMTL) was transected to destabilize the medial meniscus. The menisci were not removed. Postoperative care included the administration of analgesics and antibiotics to manage pain and prevent infections.

Animal Drug Treatment

SD rats were randomly allocated into three experimental groups: a control group (Con) that underwent no surgical intervention, an osteoarthritis model group (OA) that received DMM surgery followed by sterile saline injections, and a treatment group (Organoid@RA) that received DMM surgery followed by implantation of cartilage organoids loaded with RA (1 or 2 mg/kg) beginning two weeks post-surgery. Eight weeks after surgery, all animals were humanely euthanized and their joint tissues were harvested for comprehensive analysis. Cartilage degradation was quantitatively evaluated using the Osteoarthritis Research Society International (OARSI) scoring system, an internationally validated standard for assessing cartilage degeneration severity. Final OARSI scores for each specimen represented the mean values from three independent, blinded evaluators to ensure objective assessment of therapeutic outcomes.

Primary Chondrocyte Culture and Treatment

Primary chondrocytes were isolated from rat hip cartilage. The cartilage was diced and subjected to enzymatic digestion using 0.01 mg/mL pronase E in Dulbecco's Modified Eagle Medium (DMEM) for 30 min at 37°C, followed by 1.3 mg/mL collagenase P in chondrocyte culture medium for 16 h at 37°C. The resulting cell suspension was filtered, washed, and seeded at a density of 4×10^4 cells/cm^2. After 3 d, the medium was replaced, and cells were cultured for an additional 2 d before stimulation with rat-derived IL-1β (10 μg/mL, Sigma-Aldrich) to induce senescence. Cells in the RA group received 2 μg/mL RA after IL-1β stimulation. RNA was extracted after stimulation to assess the expression of senescence markers (*Bax, Bcl-2, Caspase-3, Cdkn2a*, and *Tnf-α*).

Immunofluorescence staining of chondrocytes primarily targeted the visualization of matrix metallopeptidase 13 (MMP13, ab52915; 1:100; Abcam) and Collagen II (ab34712; 1:100; Abcam) to assess cartilage health and remodeling processes. Initially, chondrocyte cultures were fixed with 4% paraformaldehyde and permeabilized with 0.1% Triton X-100. After blocking nonspecific binding sites with a suitable blocking solution, the cells were incubated with primary antibodies against MMP13 and Collagen II. After thorough washing, fluorescence-labeled secondary antibodies were used to detect the primary antibodies.

Synthesis and Characterization of GelMA and HAMA Hydrogels

Gelatin (5–10% w/v) was dissolved in preheated Phosphate-buffered saline (PBS) or deionized water at approximately 50°C with constant stirring. After cooling to room temperature, the pH was adjusted to 8.5 with a basic buffer. Methacrylic anhydride (MAA) was then added dropwise in two batches at MAA to gelatin amino group molar ratios of 1:10 and 4:10. The solution was stirred for 4–6 hours, maintaining a pH of 8.5. The reaction was terminated by adding excess pre-cooled PBS, followed by 5 days of dialysis to remove unreacted MAA. The resulting product was freeze-dried to obtain GelMA with varying degrees of amino substitution.

Sodium hyaluronate (HA) was dissolved in deionized water to a concentration of 1% (w/v) and stirred for approximately 6 hours until fully dissolved. The pH was adjusted to 8.5 to facilitate the reaction between HA's carboxyl groups and MAA's hydroxyl groups. In an ice bath (5°C), MAA (approximately 2 mL per gram of HA) was added dropwise over 8 hours, maintaining a pH of 8.5. The solution's pH was then adjusted to 7, and the product was dialyzed against deionized water for 3 days to remove unreacted MAA. The resulting solution was freeze-dried to obtain HAMA powder.

For RA-loaded hydrogels, RA was incorporated into the GelMA/HAMA composite system using a dissolution method. RA was first dissolved in dimethyl sulfoxide (DMSO) at a concentration of 10 mg/mL to ensure complete solubilization. The RA solution was then mixed with the GelMA/HAMA precursor solution at predetermined ratios (1–2 mg RA per gram of polymer) under gentle stirring for 30 minutes at room temperature to achieve homogeneous distribution throughout the hydrogel matrix. The RA-loaded hydrogel solution was subsequently crosslinked using UV irradiation (365 nm, 10 mW/cm^2) for 60 seconds in the presence of 0.1% (w/v) photoinitiator (Irgacure 2959).

Fourier-transform infrared (FTIR) spectroscopy was performed using a Shimadzu IRSpirit spectrometer to characterize GelMA and HAMA powders.[23] Measurements were taken in transmission mode at room temperature with KBr as background. Parameters included a signal-to-noise ratio of 30,000:1, 0.5 cm^{-1} resolution, 32 scans per minute, and a wavenumber range of 4000–400 cm^{-1}. Each spectrum accumulated 32 scans. Data processing, including absorbance/transmittance

conversion and smoothing, was done with OMNIC software. Peak fitting was performed using PeakFit 4.12 with the GaussAmp function after baseline correction and normalization.

RA release kinetics were evaluated through in vitro dissolution studies. RA-loaded hydrogel samples were immersed in PBS (pH 7.4) at 37°C with gentle agitation (100 rpm). At predetermined time intervals (1, 2, 3 and 4 weeks), aliquots were withdrawn and replaced with fresh PBS. RA concentration was quantified using UV-visible spectrophotometry at 350 nm wavelength. The release mechanism was characterized as diffusion-controlled, following Fick's second law of diffusion. Cumulative release profiles were fitted to mathematical models including zero-order, first-order, and Higuchi diffusion models to determine the release kinetics. Hydrogel degradation studies were conducted to assess the correlation between matrix degradation and RA release. RA-loaded hydrogel samples were incubated in PBS containing 1 U/mL collagenase at 37°C. Mass loss was monitored gravimetrically over 4 weeks, with samples collected at weekly intervals.

Synthesis of Cartilage Organoids

Cartilage organoids were engineered by embedding chondrocytes within layer-specific hybrid hydrogels designed to mimic native cartilage zonal properties. The construct comprised three distinct layers—superficial (S), deep (D), and subchondral bone (B)—each formulated with optimized biomaterials and bioactive factors to provide appropriate mechanical strength and biological activity.

For the superficial layer (S), hydrogels with increased mechanical strength were prepared using a mixture of 15% GelMA, 2% HAMA, and TGF-β1. RA was incorporated polymer to enhance chondrogenesis and reduce cellular senescence. This formulation targeted the thick collagen fiber matrix characteristic of the cartilage surface, ensuring sufficient compressive and tensile moduli to withstand mechanical loads.

The deep cartilage layer (D) employed a honeycomb-like hydrogel structure with 8% GelMA, 2% HAMA, and TGF-β1, supplemented with RA to maintain chondrocyte phenotype and extracellular matrix synthesis, promoting a balance between elasticity and cell viability. This layer's composition supports the typical lacunar morphology of deep chondrocytes while maintaining biomechanical compatibility.

The subchondral bone layer (B) incorporated 8% GelMA, 3% nHA, and rhBMP-2 within the hydrogel matrix to enhance stiffness and osteoinductive potential, facilitating bone regeneration and integration.

Culture and Staining of BMSC-Seeded Cartilage Organoids

Bone marrow-derived mesenchymal stem cells (BMSCs) were isolated and expanded under standard conditions in DMEM supplemented with 10% fetal bovine serum and antibiotics. Prior to seeding, BMSCs were trypsinized and resuspended at a density of 1.75×10^5 cells/mL. Cells were then seeded uniformly onto hydrogel-based scaffolds specifically designed for cartilage organoid formation. The scaffolds comprised zonal hybrid hydrogels with tailored mechanical and biological properties to mimic native cartilage layers.

Seeded constructs were cultured in a humidified incubator at 37°C with 5% CO_2. Osteogenic and chondrogenic differentiation media were applied to promote lineage-specific maturation. After 14 days, the constructs were fixed with 4% paraformaldehyde for 30 minutes at room temperature.

For immunofluorescence staining, samples were embedded and sectioned to 5–7 μm thickness. Sections were subjected to antigen retrieval before incubation with primary antibodies targeting osteocalcin (OCN, A20800, ABclonal) and aggrecan (AGG, Sc-166951, Santa), key markers for osteogenic and chondrogenic differentiation respectively. Secondary antibody incubation was performed using appropriate HRP-conjugated antibodies.

Live/Dead Cell Viability

BMSCs were seeded onto scaffolds and cultured for 7 days to assess cell viability. After culture, a Live/Dead cell viability assay was performed by staining samples with calcein-AM and propidium iodide according to the manufacturer's protocol. The scaffolds were then observed under a fluorescence microscope to visualize live (green) and dead (red) cells. Both standard photopolymerization and temperature-controlled photopolymerization curing methods were applied to the different scaffold layers (S, D, and B layers) to compare their effects on cell viability. Quantitative analysis of the fluorescence images was conducted to calculate the percentage of live cells.

Histological Analysis

Joint tissues were fixed overnight in 4% paraformaldehyde, decalcified using a decalcification solution for 28 d, and embedded in paraffin. The sections were stained with safranin O/fast green or hematoxylin and eosin (H&E).

Western Blotting Analysis

Proteins were extracted from joint tissues using radioimmunoprecipitation assay buffer. Protein concentrations were determined using a bicinchoninic acid protein assay kit. Proteins (50 μg) were separated by 12% sodium dodecyl sulfate-polyacrylamide gel electrophoresis and transferred to polyvinylidene fluoride membranes. Membranes were blocked and incubated with primary antibodies against TGFβ1 (Abcam, Cambridge, UK), Smad2 (Abmart, Shanghai, China), phospho-Smad2 (Abmart), Smad3 (Abmart), phospho-Smad3 (Abmart), and GAPDH (Santa Cruz Biotechnology), followed by horseradish-peroxidase-conjugated secondary antibodies. The bands were visualized using an enhanced chemiluminescence detection system.

Quantitative Reverse Transcription-Polymerase Chain Reaction

Total mRNA was extracted using TRIzol, and cDNA was synthesized using PrimeScript™ RT Master Mix. Quantitative reverse transcription-polymerase chain reaction (qRT-PCR) was conducted using specific primers, and gene expression levels were quantified using the $2^{-\Delta\Delta Ct}$ method, with *GAPDH* as the internal control. The qRT-PCR primers are listed in Table S1.

Statistical Analysis

Data are presented as the mean ± standard deviation (SD). Normality was assessed using the Shapiro–Wilk test. Non-normally distributed data were log-transformed for normalization. Parametric tests (paired Student's *t*-test, Welch's *t*-test, and one-way analysis of variance [ANOVA] followed by Bonferroni correction) were performed as appropriate. Statistical analyses were performed using GraphPad Prism 8.0 (GraphPad Software, San Diego, CA, USA) and R version 4.2.1 software, with Python 3.7 also utilized for statistical analysis. Statistical significance was set at $P < 0.05$.

Results

Key Regulatory Genes and Mechanisms in OA

We integrated the GSE12021, GSE55457, and GSE55235 datasets to analyze differential gene expression in cartilage and synovial tissues from patients with OA compared to healthy controls. This analysis identified 800 upregulated and 826 downregulated genes in the OA samples (Figure 2A–C). Functional enrichment analysis highlighted the significant dysregulation of pathways associated with the inflammatory response, protein secretion, phagocytosis, and ECM organization in OA samples (Figure 2D). Correspondingly, pathways related to regeneration, cell cycle regulation, aging, and cartilage morphogenesis were also significantly altered (Figure 2E). Collectively, our findings underscore the pronounced chronic inflammatory response coupled with reduced regenerative capacity in patients with OA. Disease progression was associated with cellular senescence markers, highlighting potential targets for therapeutic intervention. These results suggest that modulation of these pathways may provide new avenues for treating or potentially reversing the effects of OA.[24]

Identification of Key Senescence-Associated Genes in OA

To identify the key regulatory genes associated with OA, we employed WGCNA. By setting a stringent soft-thresholding power to achieve a scale-free topology index of $R^2 > 0.85$, we identified 11 gene modules of interest (Figure 3A–C). Notably, the brown module was most strongly correlated with the pathogenesis of OA (correlation = 0.52, $P < 0.001$). This module comprised 433 genes implicated in functions such as TNF-mediated inflammatory signaling, homeostatic regulation, lipoprotein modulation, and the dsDNA response (Figure 3D). Further analysis of genes related to cellular senescence, including both upregulated DEGs and those within the brown module, resulted in the identification of 35

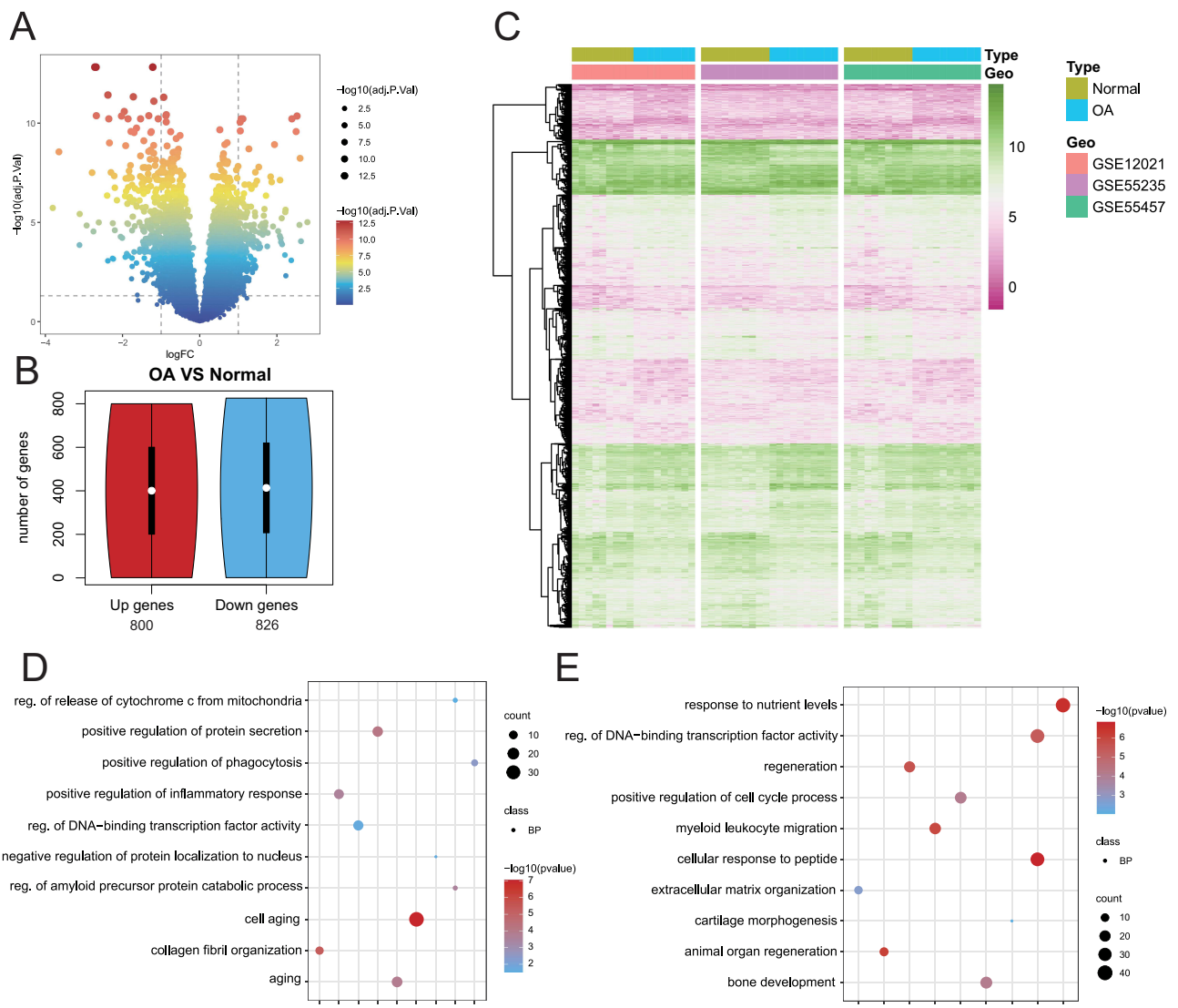

Figure 2 Identification and functional annotation of differentially expressed genes (DEGs) in OA using microarray datasets. (**A**) Volcano plots illustrating DEGs across OA datasets. Genes were filtered using a threshold of |log2(fold-change)| >0.575 and *P* <0.05. (**B**) Bar graph quantifying the number of downregulated DEGs identified in each group. (**C**) Hierarchical clustering heatmap of DEGs across three independent datasets (GSE12021, GSE55235, GSE55457), demonstrating consistent expression patterns between OA and control samples. (**D** and **E**) Enriched biological pathways derived from Gene Ontology (GO) analysis of (**D**) upregulated and (**E**) downregulated DEGs.

senescence-associated factors intimately linked with OA (Figure 3E). These factors predominantly participated in ERK pathway modulation, tissue remodeling, inflammatory response regulation, wound healing, and chemotaxis[25] (Figure 3F).

In the subsequent stage of our analysis, we employed machine learning algorithms to refine the selection of the senescence factors most relevant to OA. Using a random forest (RF) algorithm, we trained a model with performance delineated in the reverse cumulative distribution of the residuals (Figure 3G), illustrating a rapid decline in the error percentage with increasing residuals. Moreover, the error rate of the RF algorithm was inversely related to the number of decision trees. A precipitous drop in the out-of-bag error rate was observed as the number of trees approached 50 (Figure 3H). After this model optimization, we identified the following nine critical senescence factors associated with OA: *TNFRSF11B, ANGPT1, VEGFC, SERPINE1, BMP2, ANGPTL4, MMP1, EGF*, and *IGF1* (Figure 3I). These findings indicate promising targets for future therapeutic interventions.

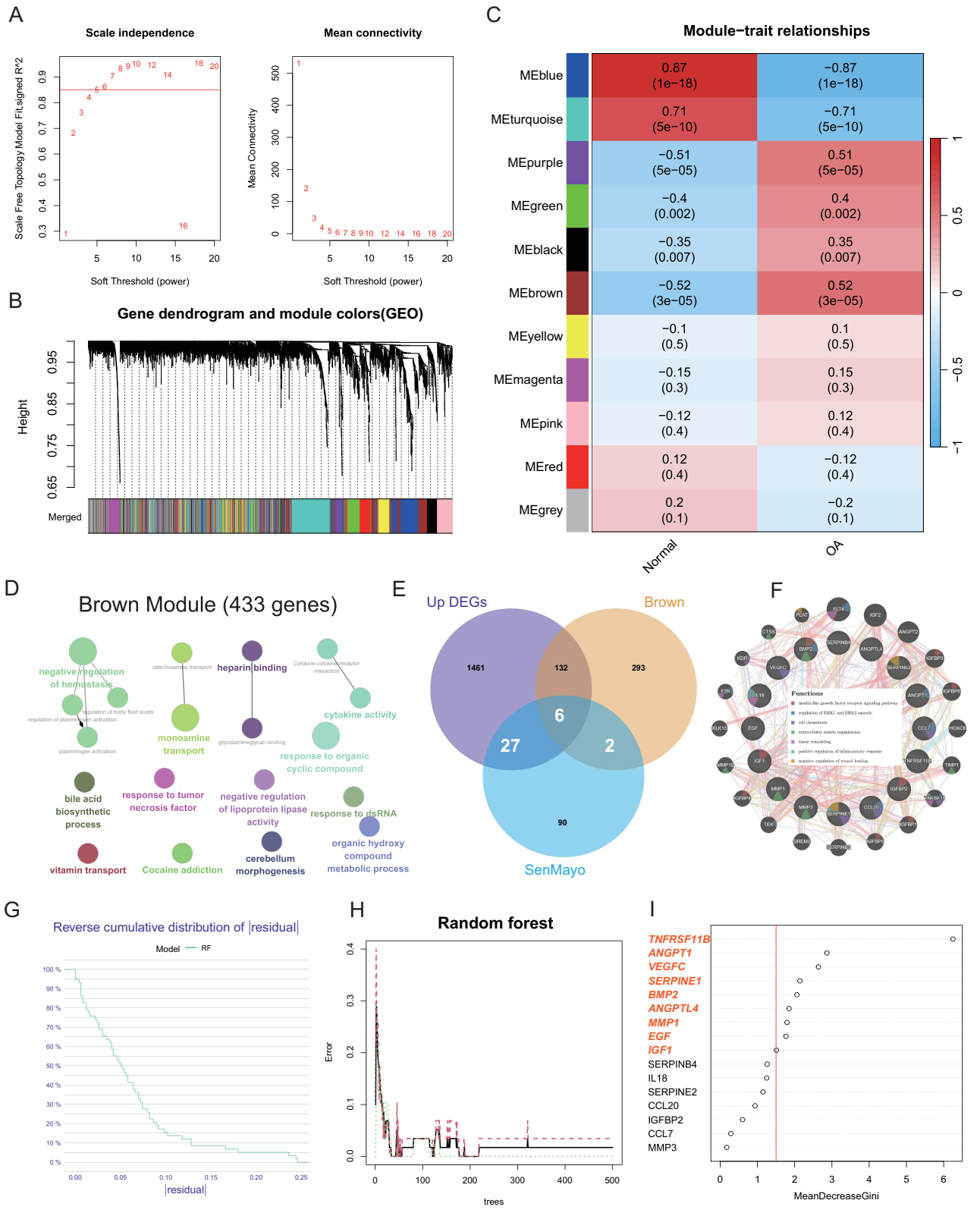

Figure 3 Identification of key senescence genes of bulk RNA-seq datasets. (**A**) Soft threshold setting according to R^2 =0.85. (**B**) The gene set is divided into 11 different modules. (**C**) The correlation of modules with OA occurrence. (**D**) Biological pathways of these brown module genes. (**E**) Venn diagram of intersected genes between DEGs, SenMayo geneset and yellow module genes. (**F**) Protein-protein interaction network of 35 key regulatory genes. (**G**) Reverse cumulative distribution of residual in RF. (**H**) Out-of-bag (OOB) error rate of RF. (**I**) Screening for key senescence genes by RF. RF: random forest.

https://doi.org/10.2147/JIR.S545622

Experimental Validation and Predictive Modeling of Key Senescence Factors in OA

After our initial screening, we employed heatmap analysis to delineate the expression profiles of nine critical senescence factors in OA and normal cartilage (Figure 4A). Notably, we observed significant upregulation of *TNFRSF11B, ANGPT1, VEGFC, MMP1, EGF*, and *IGF1*, whereas *SERPINE1, BMP2*, and *ANGPTL4* were markedly downregulated in the OA group (Figure 4B). Given the pivotal role of senescence markers in the pathogenesis of OA, we conducted qPCR validation of six significantly upregulated genes within synovial chondrocytes in a rat model of OA after eight weeks. The expression patterns of *ANGPT1, MMP1, EGF*, and *IGF1* were consistent with our transcriptome data, showing statistically significant upregulation (Figure 4C). Leveraging the expression levels of these four genes, we established

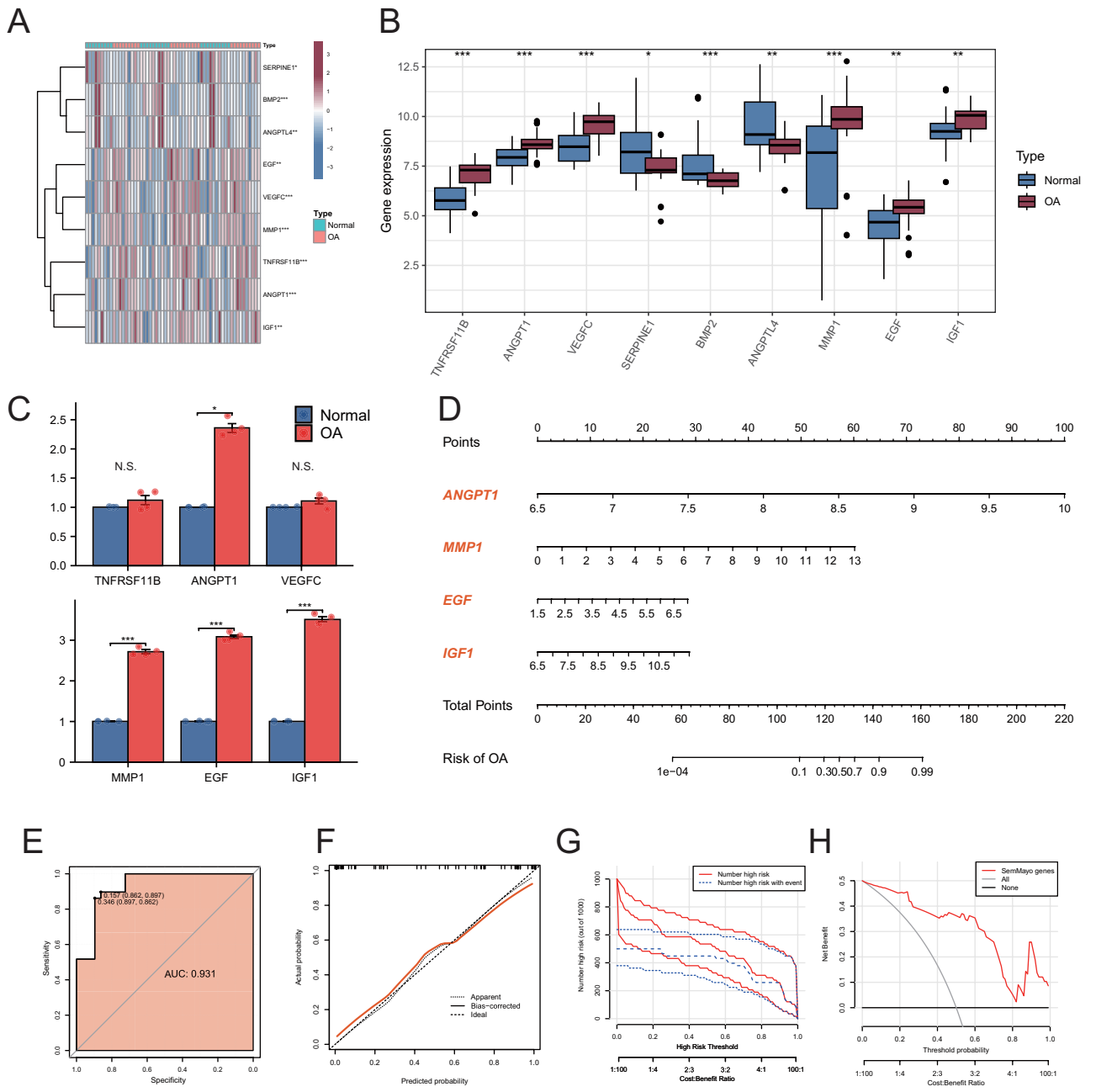

Figure 4 Experimental validation and clinical prediction models. (**A**) Heatmap of nine key senescence genes. (**B**) The differential expression of key senescence genes in bulk RNA seq between OA and normal individuals. (**C**) Validation of quantitative real-time PCR analysis. (**D**) Nomogram of key regulatory senescence genes for predicting OA. The ROC curve (**E**) Calibration curve (**F**) and Clinical decision analysis (**G** and **H**) of nomogram. **P* < 0.05, ***P* < 0.01, ****P* < 0.001.
Abbreviations: N.S., no significance.

a clinical predictive model to assess the risk of OA (Figure 4D). The robustness of our model was evidenced by both the ROC curve, which demonstrated an area under the curve (AUC) of 0.931, and the calibration curves (Figure 4E and F). Finally, the clinical utility of our predictive model was underscored using decision curve analysis and clinical benefit curves (Figure 4G and H).

Single-Cell Subpopulation Annotation and Senescence Factor Localization

Upon integrating data from the GSE169454 dataset, which encompasses cells from normal cartilage obtained during orthotopic transplantation (9,115 cells) and OA cartilage from total knee arthroplasty (66,595 cells), we identified 75,710 cells (Figure 5A). Quality control measures were implemented prior to annotating distinct cellular subpopulations within different clusters (Figure 5B). The following eight major groups were annotated: hypertrophic chondrocytes (HTCs), homeostatic chondrocytes (HomCs), cartilage progenitor cells (CPCs), pre-hypertrophic chondrocytes (preHTCs), regulatory chondrocytes (RegCs), effector chondrocytes (ECs), fibrocartilage chondrocytes (FCs), and proliferative chondrocytes (ProCs). The signature genes for each subpopulation were *WWP2, JUN, SLC4A7, S100A4, ATOX1, DSC2,*

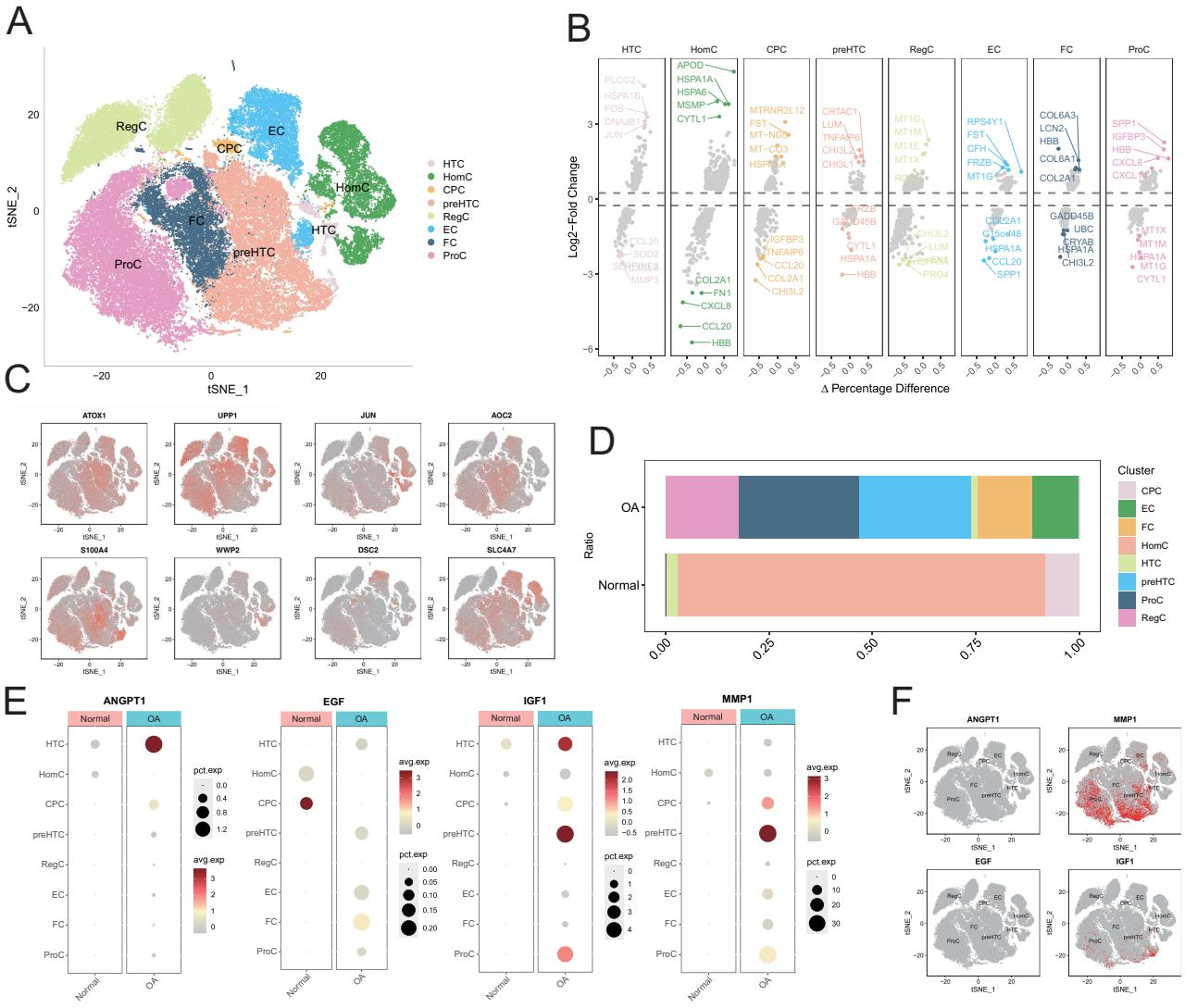

Figure 5 Single cell sequencing of Osteoarthritis. (**A**) The t-SNE plot of multiple cell types from healthy and osteoarthritis (OA) groups. (**B**) Marker genes of eight types of chondrocytes. (**C**) Characteristic marker genes of eight types of chondrocytes. (**D**) Proportions of eight types of chondrocytes in different cell types. (**E**) Expression levels of four key aging-related genes across chondrocyte subtypes. (**F**) t-SNE plots depicting the spatial distribution of the four key aging-related genes.

https://doi.org/10.2147/JIR.S545622

AOC2, and *UPP1*, respectively (Figure 5C). Notably, post-OA analysis revealed a significant decrease in the number of HomCs and CPCs and an increase in the number of all other subpopulations, with the exception of HTCs (Figure 5D).

Further examination of senescence factors at the single-cell level post-OA showed that *ANGPT1* expression levels were significantly elevated in all subpopulations, except HomCs. *EGF* levels increased in all cells except HomCs and CPCs. *IGF1* was markedly upregulated across all subpopulations, and *MMP1* expression levels were significantly higher mainly in CPCs and preHTCs (Figure 5E and F). Collectively, these findings suggest that in accordance with bulk transcriptome predictions, key senescence factors are upregulated to various extents in OA-affected cells, with the exception of HomCs and CPCs.

Identification of Key Senescent Cells and Potential Regulatory Pathways in OA

To elucidate the differentiation trajectories and directions of various cells in OA, we performed a pseudo-time analysis on all sampled cells. Using Monocle 2, we determined that post-OA cell subpopulations predominantly differentiated from normal cartilage cells (Figure 6A and B). Further sub-clustering analysis indicated that HomCs and HTCs represented the initial states of differentiation, while RegCs and FCs were identified as terminal states of distinct differentiation pathways, with other cells occupying intermediate transitional states (Figure 6C). Subsequently, the senescence index of all cells was quantified using the Senmyao gene set, revealing that, compared to HomCs, other cell types exhibited significantly increased senescence scores, with ProCs, FCs, and preHTCs showing a marked elevation (Figure 6D and E).

Cell-cell communication between normal and OA cells was also examined. In the normal set, HomCs exhibited the strongest interaction network, whereas in the OA set, ECs displayed more potent interactions (Figure 6F). Upon further analysis of interactions involving HomCs, a conspicuous downregulation of the TGFβ signaling pathway was observed (Figure 6G). Overall, the TGFβ signaling pathway was most prominently involved in the communication between HomCs and both preHTCs and ECs (Figure 6H). The ligand-receptor interactions involving TGFβ1 and its receptors TGFβR1, TGFβR2, and ACVR1 were identified as key regulatory pathways in OA (Figure 6I). In summary, we believe that the TGF β signaling pathway is a key pathway regulating the interaction between HomCs and these key senescent OA subpopulations.

Prediction of Potential Pharmacological Modulators of Cellular Senescence

To identify potential compounds for modulating four senescence-related proteins, we utilized the DSigDB database and identified RA as a promising candidate for targeting key senescence-related genes involved in OA ($P = 0.002$, combined score = 62,968). To further investigate this, we employed AutoDock software to predict potential binding sites of RA with senescence-associated proteins: ANGPT1, MMP1, EGF, and IGF1. The predicted binding energies for RA binding to these proteins were as follows: ANGPT1 (−5.386 kcal/mol), MMP1 (−5.923 kcal/mol), EGF (−5.039 kcal/mol), and IGF1 (−5.140 kcal/mol), suggesting a strong binding affinity between RA and these senescence-related proteins (Figure 7A–D).

To further assess the stability and dynamics of RA's interaction with these proteins in vivo, we employed molecular dynamics simulations to evaluate the binding stability, flexibility, and dynamic behavior of RA-protein complexes. Root means square deviation (RMSD), a well-established indicator of protein-ligand stability, was used to assess the equilibrium of the system. A lower RMSD value suggests greater conformational stability. As shown in Figure 7E, the RMSD for the IL18-docking complex reached equilibrium at 98 ns, with a final fluctuation of approximately 1.6 Å. The BMP2-docking complex achieved equilibrium at 98 ns with a final fluctuation of 3.6 Å. The IGFBP2-docking complex stabilized at 98 ns with a fluctuation of 18.7 Å, while the SERPINE1-docking complex achieved equilibrium at 98 ns with a final fluctuation of 2.1 Å. Notably, the IL18-docking complex exhibited the lowest RMSD, suggesting a higher stability in the RA-IL18 interaction. Further analysis of the radius of gyration (Rg) and solvent-accessible surface area (SASA) during the simulation revealed slight fluctuations in the IL18-docking, BMP2-docking, IGFBP2-docking, and SERPINE1-docking complexes (Figure 7F and G). These fluctuations indicate conformational changes during the simulation, with the RA binding sites on these proteins undergoing minor structural adjustments.

Hydrogen bonding plays a crucial role in the binding of ligands to their target proteins. As depicted in Figure 7H, the number of hydrogen bonds between the RA molecule and target proteins varied during the simulation. The IL18-docking complex formed between 0 and 3 hydrogen bonds, with an average of approximately 2 hydrogen bonds. The BMP2-

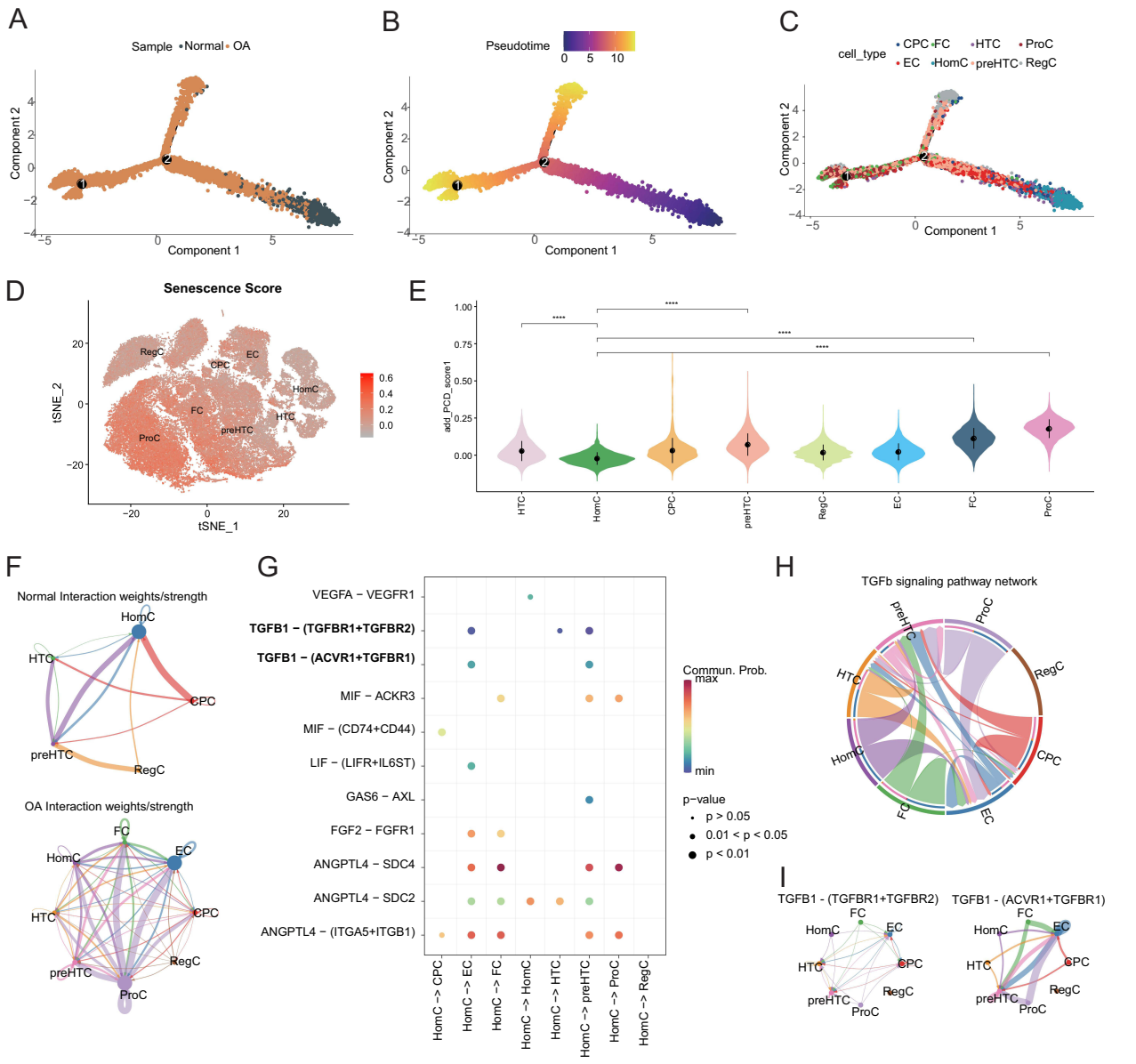

Figure 6 Identification of Key Senescent Cells and Potential Regulatory Pathways in Osteoarthritis: (**A**) UMAP visualization of chondrocyte populations colored by sample origin (Normal vs OA - osteoarthritis). Two distinct trajectory branches are indicated by numbered arrows (1 and 2), suggesting divergent developmental pathways in normal and osteoarthritic conditions. (**B**) Pseudotime trajectory analysis showing the temporal progression of chondrocyte differentiation. (**C**) Cell type annotation overlay showing the distribution of eight distinct chondrocyte subtypes along the pseudotime trajectories: OPC. (**D**) Senescence scoring of chondrocytes. (**E**) Violin plot of senescence scores in chondrocytes. (**F**) Cell-cell communication analysis in chondrocytes. (**G**) Cell-cell communication between HomoC and other chondrocyte types. (**H** and **I**) Role of the TGFβ signaling pathway in various chondrocyte types. ****$P < 0.0001$.

docking complex exhibited 0 to 7 hydrogen bonds, with an average of around 3 hydrogen bonds. The IGFBP2-docking complex formed between 0 and 4 hydrogen bonds, with an average of 2 hydrogen bonds. Similarly, the SERPINE1-docking complex exhibited 0 to 3 hydrogen bonds, with an average of 2 hydrogen bonds. These findings indicate that RA forms stable hydrogen bond interactions with these senescence-related proteins. Additionally, the root mean square fluctuation (RMSF), which reflects the flexibility of the amino acid residues in the proteins, was measured (Figure 7I–L). The RMSF values for the IL18-docking, BMP2-docking, IGFBP2-docking, and SERPINE1-docking complexes were relatively low (mostly below 4 Å), indicating that the complexes maintain low flexibility and high stability during the simulation.

In summary, the IL18-docking, BMP2-docking, IGFBP2-docking, and SERPINE1-docking complexes exhibited stable binding interactions with RA. The IL18-docking complex, in particular, demonstrated a low RMSD value and

https://doi.org/10.2147/JIR.S545622

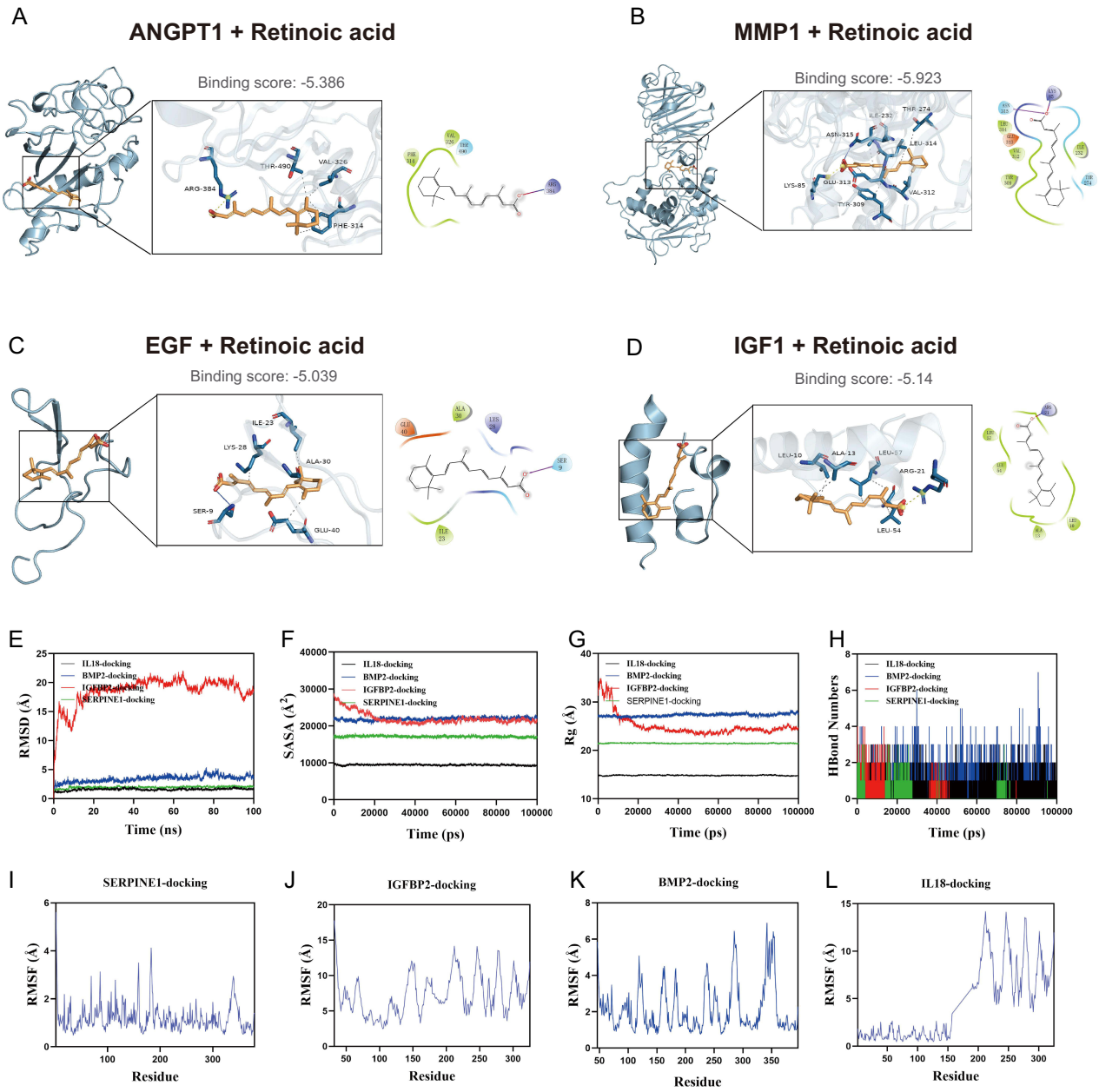

Figure 7 Prediction of Potential Pharmacological Modulators of Cellular Senescence. (**A**–**D**) Molecular docking schematic diagrams illustrating the potential binding sites of decitabine with ANGPT1, MMP1, EGF, and IGF1 proteins. In these panels, the proteins are displayed in cartoon representation, with blue stick models representing amino acid residues and the small molecule decitabine shown in yellow. Blue solid lines indicate hydrogen bonds, whereas gray dashed lines represent hydrophobic interactions. (**E**) RMSD profiles for four protein–ligand (RA) complexes, demonstrating the stability of the complexes over the simulation period. (**F**) SASA analysis for the four protein–ligand (RA) complexes, reflecting the extent of solvent exposure. (**G**) Rg values of the four protein–ligand (RA) complexes, indicating the overall compactness of the binding systems. (**H**) Quantification of the number of hydrogen bonds formed in the four protein–ligand (RA) complexes. (**I**–**L**) RMSF analyses for the IL18-docking, BMP2-docking, IGFBP2-docking, and SERPINE1-docking complexes, respectively, highlighting the dynamic flexibility of the protein regions upon ligand binding.

strong hydrogen bond interaction, suggesting a highly stable and favorable binding between RA and the senescence-related target proteins.

Attenuation of Chondrocyte Senescence by RA

Primary chondrocytes treated with IL-1β were utilized to simulate the senescence-associated phenotype typical in the pathogenesis of OA.[26] After treatment, we quantitatively assessed the expression of apoptosis-related genes. qRT-PCR analysis revealed that RA treatment significantly decreased the expression levels of key apoptotic markers including *Bax,*

Bcl-2, and *caspase-3* (Figure 8A). Concurrently, Western blotting indicated that TGF-β1, phosphorylated Smad2, and phosphorylated Smad3 were upregulated in the RA-treated groups, suggesting activation of the TGFβ1/Smad signaling pathway (Figure 8B). In summary, our results indicate that RA can ameliorate IL-1β-induced chondrocyte apoptosis through the activation of the TGF-β signaling pathway.

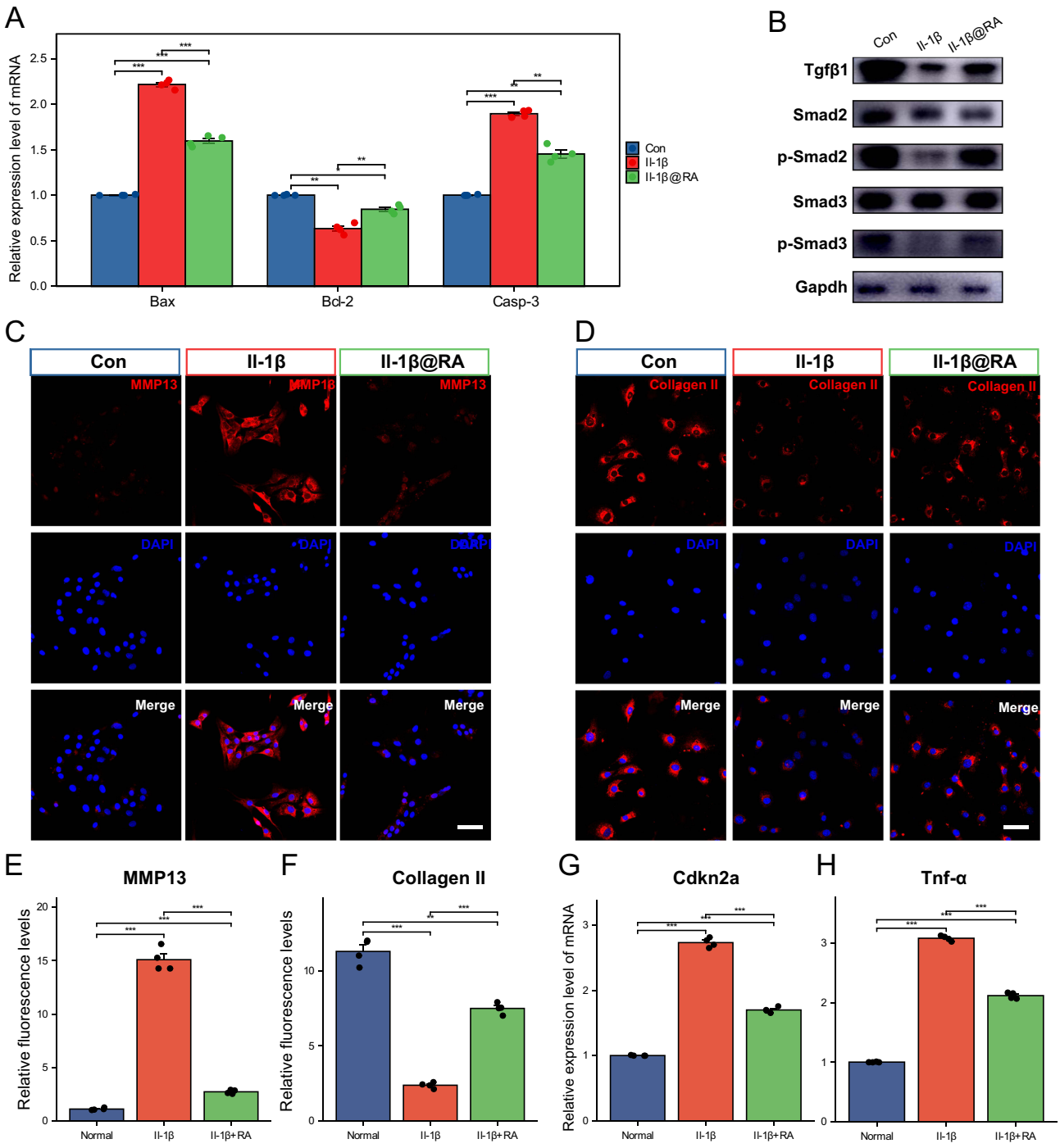

Figure 8 In vitro functional and histological assessment of RA. (**A**) Quantitative PCR analysis of the expression levels of three key apoptotic factors in three groups of chondrocytes (Con, IL-1β, IL-1β@RA). (**B**) Expression levels of key proteins in the TGFβ/Smad signaling pathway in three groups of chondrocytes. (**C–F**) Expression levels of MMP13 and Collagen II in three groups of chondrocytes, scale bar = 40um. (**G** and **H**) Quantitative PCR analysis of the expression levels of *Cdkn2a, Tnf-α*. Statistical significance was determined using one-way ANOVA followed by Bonferroni correction. **P* < 0.05, ***P* < 0.01, ****P* < 0.001.

https://doi.org/10.2147/JIR.S545622

In relation to ECM components, senescent chondrocytes exhibited reduced collagen II levels and increased MMP13 levels. However, RA treatment effectively reversed these trends, as demonstrated in immunofluorescence (Figure 8C–F). Furthermore, we evaluated the expression of SASP factors, specifically *Cdkn2a* and *Tnf-α* (Figure 8G and H). Our findings showed that RA treatment ameliorated the upregulation of these markers, underscoring its potential in mitigating SASP-mediated effects in chondrocyte senescence.

Triphasic Organoids@OA Mitigate Chondrocyte Senescence

To enhance the attenuation of chondrocyte senescence by RA in vivo, we developed a triphasic cartilage organoid system based on GelMA/HAMA composite hydrogels. By dual modulation of amine substitution degree and polymer concentration, we achieved differential release profiles of RA and TGF-β1, enabling spatially controlled delivery of bioactive factors within the construct (Figure 9A). FTIR analysis of GelMA samples revealed consistent characteristic peaks among variants, with the absorption peak at 3277 cm^{-1} corresponding to hydroxyl and N–H stretching vibrations showing a redshift indicative of strengthened intermolecular hydrogen bonding (Figure 9B). Another peak at 3069 cm^{-1} was assigned to the amide B band involving amide N–H and unsaturated C–H stretching modes (Figure 9B). Finally, optimal synthesis conditions for GelMA (50 °C, pH 8.5–9, 180 min, MA:Gelatin ratio of 10–25%) and HAMA (55 °C, pH 8.5, 24 h stirring, MA:HA = 1:2) were established to ensure reproducible biomaterial properties. To guarantee structural stability and uniform polymerization, each layer underwent temperature-controlled photopolymerization. Live/dead staining of BMSCs co-cultured with these hydrogels showed that temperature-regulated curing did not compromise cell viability, supporting cell-friendly fabrication conditions (Figure 9C and D).

During co-culture experiments, the cartilage organoids demonstrated an intrinsic capacity to promote BMSC osteogenic differentiation, as indicated by increased osteocalcin protein expression and upregulated mRNA levels (Figure 9E and F). To optimize RA delivery, we evaluated two RA concentrations (1 and 2 mg/g) within the organoid system. Mechanical characterization revealed that RA-loaded organoids (1 and 2 mg/g) maintained comparable compressive moduli to unloaded controls, indicating that drug incorporation did not compromise structural integrity (Figure S1A). Comparative analysis revealed that 2 mg/g RA-loaded organoids exhibited superior long-term release kinetics ($P < 0.05$) coupled with reduced degradation rates ($P < 0.05$) compared to the lower concentration formulation (Figure S1B and C). Additionally, 2 mg/g RA-loaded organoids significantly ameliorated SASP markers in aged chondrocytes, as evidenced by reduced Bax and Caspase-3 expression, while enhancing extracellular matrix homeostasis through increased Collagen II expression and decreased MMP13 levels over a four-week period (Figure S1C and D). Based on these release-degradation profiles and biological efficacy data, subsequent experiments employed the 2 mg/g RA concentration. Subsequently, both the deep layer honeycomb structure (organoid 1) and surface layer spiderweb architecture (organoid 2) significantly enhanced Aggrecan protein and gene expression in BMSCs, indicative of chondrogenic differentiation (Figure 9G and H). Notably, the organoid 1 formulation loaded with RA exhibited a markedly stronger pro-chondrogenic effect compared to non-RA controls, underscoring the role of RA in potentiating chondrogenesis within the organoid microenvironment (Figure 9G and H).

To evaluate the in vivo therapeutic efficacy of RA-loaded cartilage organoids, the constructs were implanted into a DMM rat model two weeks post-surgery (Figure 9I). Compared to untreated OA controls, the group treated with RA-loaded cartilage organoids demonstrated a significant reduction in cartilage degeneration severity. This was clearly demonstrated by markedly lower OARSI scores in the RA-loaded organoid groups, especially in the 2 mg/g RA group, which showed the most significant improvement ($P < 0.001$, Figure 9J). Histological analysis performed eight weeks after implantation using H&E and Safranin O/fast green staining further confirmed improved cartilage preservation in the RA group. Specifically, treated joints showed a smoother cartilage surface, more integrated tissue architecture, and increased cartilage thickness, indicative of effective regenerative repair (Figure S1E). Together, these findings indicate that RA-loaded GelMA/HAMA cartilage organoids substantially mitigate cartilage degeneration and hold promise as a potential therapeutic strategy for osteoarthritis (Figure 9K).

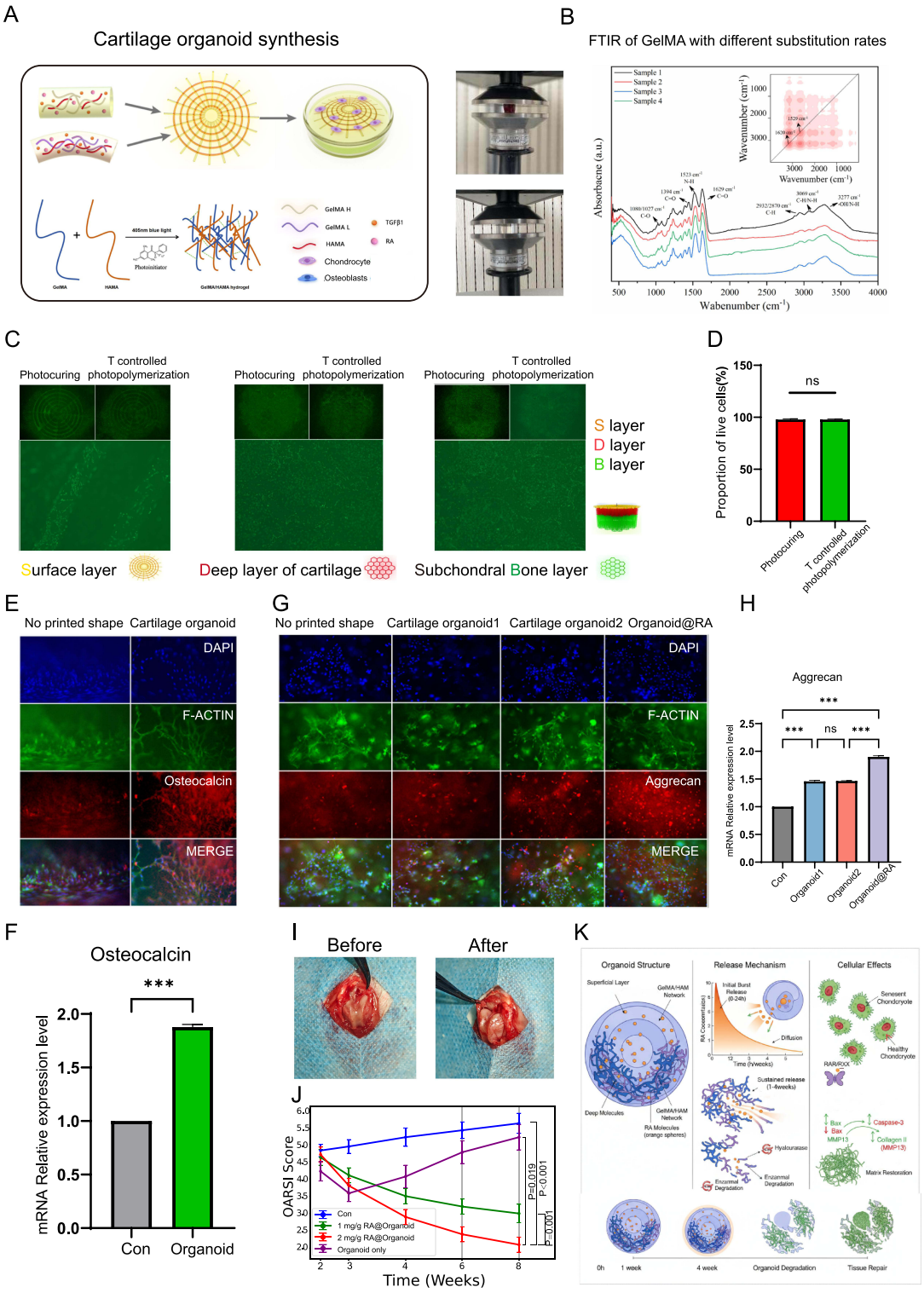

Figure 9 Triphasic GelMA/HAMA Cartilage Organoids with RA for Attenuating Chondrocyte Senescence and Promoting Cartilage Repair in Osteoarthritis. (**A**) Schematic illustration of the triphasic cartilage organoid synthesis process, showcasing the dual modulation of amine substitution degree and polymer concentration for controlled release of retinoic acid (RA) and TGF-β1. (**B**) FTIR spectra of GelMA samples, highlighting characteristic peaks at 3277 cm^{-1} (hydroxyl and N–H stretching, redshifted due to enhanced hydrogen bonding) and 3069 cm^{-1} (amide B band, N–H and unsaturated C–H stretching). (**C** and **D**) Live/dead staining of BMSCs co-cultured with organoids, demonstrating maintained cell viability post-temperature-controlled photopolymerization. (**E**) Immunofluorescence analysis showing increased osteocalcin expression in BMSCs, indicative of osteogenic differentiation. (**F**) Quantitative PCR analysis of the expression levels of *osteocalcin*. (**G**) Enhanced Aggrecan protein expression of immunofluorescence in organoid 1 (honeycomb) and organoid 2 (spiderweb), with RA-loaded organoid 1 exhibiting superior chondrogenic effects. (**H**) Quantitative PCR analysis of the expression levels of *Aggrecan*. (**I**) Implantation of RA-loaded organoids into a DMM rat model at two weeks post-surgery. (**J**) OARSI score comparison of different treatment groups over 8 weeks. (**K**) Schematic illustration of organoid-based drug delivery system for osteoarthritis treatment. **P* < 0.05, ***P* < 0.01, ****P* < 0.001.

https://doi.org/10.2147/JIR.S545622

Discussion

OA is a chronic degenerative joint disease intricately linked to aging.[27] Understanding the molecular mechanisms by which aging contributes to OA progression is critical for deciphering its pathophysiology. Among the nine hallmarks of aging identified across species, tissues, and cells, cellular senescence has emerged as a central driver of OA progression and exacerbation.[28] In this study, we leveraged microarray and scRNA-seq data to map the aging landscape in OA, identifying critical senescence-related genes and pathways that exacerbate disease progression. Our findings highlight the therapeutic potential of RA in modulating the TGFβ signaling pathway, a key regulator of cellular aging, to mitigate OA progression by managing chondrocyte senescence and restoring cartilage integrity. These insights underscore the importance of targeting aging processes in OA and provide a foundation for future clinical trials to validate the efficacy and safety of RA as a therapeutic intervention.

We identified pivotal senescence-associated genes—*ANGPT1, MMP1, EGF, and IGF1*—each of which has been previously reported to contribute distinctly to OA pathogenesis. Among these, *ANGPT1* enhances synovial inflammation and induces vascular alterations, suggesting that targeting angiogenesis could alleviate disease severity.[29] *MMP1*, a key mediator of collagen degradation, plays a central role in cartilage breakdown, rendering it a promising therapeutic target.[30] In contrast, although *EGF* exhibits chondroprotective properties under certain conditions, it paradoxically exacerbates cartilage destruction by stimulating matrix metalloproteinases, underscoring the necessity for precise modulation of its activity.[31] Moreover, while *IGF1* exerts a protective effect on cartilage during the early stages of OA, it may promote aberrant cartilage calcification in later stages, thereby exacerbating cartilage damage.[32] Collectively, these results indicate that targeting these key senescence-associated factors could ameliorate OA symptoms and offer promising avenues for novel therapeutic interventions.

In the progression of OA, different subtypes of chondrocyte cells perform distinct functions, and scRNA-seq analysis revealed the heterogeneity of chondrocyte populations and their unique roles in cartilage dynamics and OA pathology. Previous studies have shown that HomCs maintain matrix homeostasis, but their function is compromised in OA, contributing to cartilage degradation. ProCs and CPCs face significant regenerative challenges in the inflammatory environment of OA.[19,33] Our study further supports these findings, with pseudo-time analysis demonstrating a transition of chondrocyte cells from HomCs to states with elevated senescence scores. This transition underscores the critical role of cellular aging in the progression of OA, highlighting the dynamic shifts that occur within the chondrocyte populations as the disease advances.

Central to our findings is the pivotal role of the TGF-β1 signaling pathway in modulating chondrocyte senescence. In healthy joints, TGF-β1 signaling promotes cartilage integrity and suppresses inflammation.[34] However, in OA, disrupted TGF-β1 signaling contributes to disease progression through enhanced cartilage degradation and synovial inflammation. Receptor-mediated activation of TGF-β1, primarily through type I and II serine/threonine kinase receptors, triggers SMAD-dependent pathways that are essential for cellular responses.[14] The imbalance in TGF-β1 signaling in OA suggests that therapeutic modulation of this pathway could restore the functional homeostasis of the osteoarthritic joint. By targeting this pathway, it may be possible to mitigate cartilage degradation and inflammatory responses, offering a promising avenue for OA treatment.

Our in vitro IL-1β chondrocyte model isolates a defined catabolic/senescent stimulus and does not capture synovitis, immune-cell infiltration, or dynamic loading present in vivo.[26] These factors can shift RA signaling through RAR/RXR and its crosstalk with NF-κB and TGF-β/Smad pathways, and synovial clearance may lower free RA levels. The sustained-release organoid is intended to buffer these effects by maintaining intra-cartilage RA. Accordingly, our data should be viewed as proof-of-concept for an RA delivery platform; comprehensive mapping of microenvironmental signaling will be pursued in synovium–cartilage co-culture/ex vivo models.

Current OA treatments, including nonpharmacological interventions, pharmacotherapy, and surgery, have significant limitations.[35] Long-term use of nonsteroidal anti-inflammatory drugs, for instance, is associated with gastrointestinal, cardiovascular, and renal risks. Our findings suggest that RA holds therapeutic promise due to its dual modulatory effects on inflammation and cartilage repair. RA enhances the synthesis of key matrix components, such as collagen II and aggrecan, supports chondrocyte proliferation, and reduces apoptosis, addressing the degenerative nature of OA.[36]

The development of GelMA/HAMA cartilage organoids represents a potential transformative approach to address chondrocyte senescence in OA, a chronic degenerative joint disease driven by cellular aging and inflammation.[37,38] Our triphasic organoid system, designed to mimic the native cartilage architecture, facilitates spatially controlled release of RA and TGF-β1, overcoming the limitations of conventional drug delivery methods, such as rapid clearance and poor joint retention. Unlike two-dimensional cultures, these three-dimensional constructs preserve critical cell-cell and cell-matrix interactions, which are essential for maintaining chondrocyte phenotype and function, as supported by prior studies demonstrating enhanced chondrogenic differentiation in 3D microenvironments. The organoids' ability to modulate the TGF-β1 signaling pathway, identified in our scRNA-seq analysis as disrupted in senescent chondrocytes, aligns with reports that 3D systems restore TGF-β responsiveness, reducing catabolic activity and promoting ECM synthesis. The biomimetic mechanical properties of our organoids provide mechanotransduction cues that mitigate SASP effects, consistent with evidence that appropriate mechanical stimuli influence chondrocyte behavior. Significant improvements in cartilage integrity and reduced OARSI scores in our in vivo model corroborate findings that biomimetic scaffolds enhance cartilage repair. Collectively, these results position RA-loaded GelMA/HAMA organoids as a promising candidate for disease-modifying therapy for OA, warranting further preclinical validation and clinical exploration.

Several limitations should be acknowledged. First, in vivo evaluation was limited to 8 weeks post-DMM surgery. While no adverse events or synovitis were observed, long-term outcomes beyond 4 months remain unknown. Second, the small sample size (n=3 per group) may reduce statistical power for detecting differences in OARSI scoring. Larger cohorts would strengthen confidence in translational potential. Third, the DMM model primarily reflects post-traumatic OA and may not capture age-related OA characteristics where inflammaging could alter RA signaling efficacy. Fourth, comprehensive in vivo mechanistic analyses were not performed, specifically omitting quantification of SASP factors and TGF-β/Smad pathway activation in joint tissues, which limits tissue-level mechanistic resolution. Future studies will address these limitations through longitudinal profiling of inflammatory markers and RA pharmacokinetics in synovial fluid.

Conclusions

Through single-cell transcriptomic analysis, we identified key senescence-associated genes and dysregulated TGF-β signaling as central drivers of chondrocyte senescence in OA, leading to the selection of retinoic acid (RA) as a therapeutic candidate. RA-loaded, triphasic GelMA/HAMA cartilage organoids provide controlled, localized retinoic acid delivery that attenuates chondrocyte senescence via TGFβ/Smad signaling and restores matrix homeostasis. In a rat DMM model, this platform mitigated cartilage degeneration and improved tissue architecture. These results position RA-organoids as a disease-modifying strategy for osteoarthritis with translational potential.

Abbreviations

OA, osteoarthritis; ECM, extracellular matrix; TGF-β, transforming growth factor-β; WGCNA, weighted gene co-expression network analysis; RA, retinoic acid; DMM, destabilization of the medial meniscus; SASP, senescence-associated secretory phenotype; NF-κB, nuclear factor kappa B; scRNA-seq, Single-cell RNA sequencing; GelMA, gelatin methacryloyl; HAMA, hyaluronic acid methacryloyl; DEGs, differentially expressed genes; TOM, topological overlap matrix; PCA, principal component analysis; t-SNE, t-distributed stochastic neighbor embedding; SD, Sprague-Dawley; MMTL, medial meniscotibial ligament; OARSI, Osteoarthritis Research Society International; DMEM, Dulbecco's Modified Eagle Medium; PBS, phosphate-buffered saline; DMSO, dimethyl sulfoxide; FTIR, fourier-transform infrared; TGF-β1, transforming growth factor-beta 1; BMSCs, bone marrow-derived mesenchymal stem cells; OCN, osteocalcin; AGG, aggrecan; MMP13, matrix metallopeptidase 13; H&E, hematoxylin and eosin; qRT-PCR, quantitative reverse transcription-polymerase chain reaction; ANOVA, analysis of variance; RF, random forest; ROC, receiver operating characteristic; HTCs, hypertrophic chondrocytes; HomCs, homeostatic chondrocytes; CPCs, cartilage progenitor cells; preHTCs, pre-hypertrophic chondrocytes; RegCs, regulatory chondrocytes; ECs, effector chondrocytes; FCs, fibrocartilage chondrocytes; ProCs, proliferative chondrocytes; RMSD, root mean square deviation; SASA, solvent-accessible surface area; Rg, radius of gyration; RMSF, root mean square fluctuation.

Data Sharing Statement

The datasets (GSE12021, GSE55457, GSE169454, and GSE55235) used in this study can be found in the Gene Expression Omnibus database (http://www.ncbi.nlm.nih.gov/geo/).

Ethics Approval and Informed Consent

The animal study protocol was approved by the Animal Research Ethics Committee of Fourth Military Medical University, Xi'an, China (license no. IACUC-20241366) and was performed in accordance with the National Standard for Laboratory Animal Welfare of China (GB/T 35892-2018).

Funding

This work was supported by National Natural Science Foundation of China (Grant No. 82572831).

Disclosure

The authors declare that the research was conducted in the absence of any commercial or financial relationships that could be construed as a potential conflict of interest.

References

1. Cross M, Ong KL, Culbreth GT. Global, regional, and national burden of gout, 1990–2020, and projections to 2050: a systematic analysis of the Global Burden of Disease Study 2021. *Lancet Rheumatol*. 2024;6(8):e507–e517. doi:10.1016/S2665-9913(24)00117-6
2. Rhon DI, Kim M, Asche CV, Allison SC, Allen CS, Deyle GD. Cost-effectiveness of physical therapy vs intra-articular glucocorticoid injection for knee osteoarthritis: a secondary analysis from a randomized clinical trial. *JAMA Network Open*. 2022;5(1):e2142709. doi:10.1001/jamanetworkopen.2021.42709
3. Richard MJ, Driban JB, McAlindon TE. Pharmaceutical treatment of osteoarthritis. *Osteoarthritis Cartilage*. 2023;31(4):458–466. doi:10.1016/j.joca.2022.11.005
4. Abramoff B, Caldera FE. Osteoarthritis: pathology, diagnosis, and treatment options. *Med Clin North Am*. 2020;104(2):293–311. doi:10.1016/j.mcna.2019.10.007
5. Zhong F, Cen S, Long C, Teng L, Zhong G. SIRT2 alleviates inflammatory response, apoptosis, and ECM degradation in osteoarthritic chondrocytes by stabilizing PCK1. *Discov Med*. 2024;36(189):2046–2054. doi:10.24976/Discov.Med.202436189.188
6. Han Z, Wang K, Ding S, Zhang M. Cross-talk of inflammation and cellular senescence: a new insight into the occurrence and progression of osteoarthritis. *Bone Res*. 2024;12(1):69. doi:10.1038/s41413-024-00375-z
7. Lan YY, Heather JM, Eisenhaure T, et al. Extranuclear DNA accumulates in aged cells and contributes to senescence and inflammation. *Aging Cell*. 2019;18(2):e12901. doi:10.1111/acel.12901
8. Loeser RF, Collins JA, Diekman BO. Ageing and the pathogenesis of osteoarthritis. *Nat Rev Rheumatol*. 2016;12(7):412–420. doi:10.1038/nrrheum.2016.65
9. Ran J, Ma C, Xu K, et al. Schisandrin B ameliorated chondrocytes inflammation and osteoarthritis via suppression of NF-κB and MAPK signal pathways. *Drug Des Devel Ther*. 2018;12:1195–1204. doi:10.2147/DDDT.S162014
10. Boer CG, Yau MS, Rice SJ, et al. Genome-wide association of phenotypes based on clustering patterns of hand osteoarthritis identify WNT9A as novel osteoarthritis gene. *Ann Rheum Dis*. 2021;80(3):367–375. doi:10.1136/annrheumdis-2020-217834
11. Gu Y, Jin Q, Hu J, et al. Causality of genetically determined metabolites and metabolic pathways on osteoarthritis: a two-sample mendelian randomization study. *J Transl Med*. 2023;21(1):357. doi:10.1186/s12967-023-04165-9
12. Chen Y, Lin J, Shi D, et al. Identification of WDR74 and TNFRSF12A as biomarkers for early osteoarthritis using machine learning and immunohistochemistry. *Front Immunol*. 2025;16:1517646. doi:10.3389/fimmu.2025.1517646
13. Zhou J, Jiao S, Huang J, et al. Comprehensive analysis of programmed cell death-related genes in diagnosis and synovitis during osteoarthritis development: based on bulk and single-cell RNA sequencing data. *J Inflamm Res*. 2025;18:751–778. doi:10.2147/JIR.S491203
14. Zhang Z, Li X, Guo W, Huang Z. Enhancing GFPT1 expression with glutamine protects chondrocytes in osteoarthritis. *Int Immunopharmacol*. 2024;143(Pt 2):113427. doi:10.1016/j.intimp.2024.113427
15. Bai L, Zhou D, Li G, Liu J, Chen X, Su J. Engineering bone/cartilage organoids: strategy, progress, and application. *Bone Res*. 2024;12(1):66. doi:10.1038/s41413-024-00376-y
16. Zeng D, Chen Y, Liao Z, et al. Cartilage organoids and osteoarthritis research: a narrative review. *Front Bioeng Biotechnol*. 2023;11:1278692. doi:10.3389/fbioe.2023.1278692
17. Ge YS, Ding JY, Shen J, et al. Progress in antisenescence biomaterials for improved osteoarthritis therapy. *Acta Biomater*. 2025;205:81–104. doi:10.1016/j.actbio.2025.08.044
18. Saul D, Kosinsky RL, Atkinson EJ, et al. A new gene set identifies senescent cells and predicts senescence-associated pathways across tissues. *Nat Commun*. 2022;13(1):4827. doi:10.1038/s41467-022-32552-1
19. Fu W, Hettinghouse A, Chen Y, et al. 14-3-3 epsilon is an intracellular component of TNFR2 receptor complex and its activation protects against osteoarthritis. *Ann Rheum Dis*. 2021;80(12):1615–1627. doi:10.1136/annrheumdis-2021-220000
20. Cheng J, He Z, Liu Y, Jing J, Zhang H. Integrating machine learning and multi-omics to identify key SUMOylation molecular signature in sarcoma. *Life Conflux*. 2024;1(1):e88. doi:10.71321/lcflx.00001

21. Yu B, Zhang Y, Yang Y, et al. Neonatal-inspired reprogramming of microglial pan-programmed cell death enhances regeneration in adult spinal cord injury. *Research*. 2025;8:0759. doi:10.34133/research.0759
22. Jo S, Kim T, Iyer VG, Im W. CHARMM-GUI: a web-based graphical user interface for CHARMM. *J Comput Chem*. 2008;29(11):1859–1865. doi:10.1002/jcc.20945
23. Greife P, Schönborn M, Capone M, et al. The electron-proton bottleneck of photosynthetic oxygen evolution. *Nature*. 2023;617(7961):623–628. doi:10.1038/s41586-023-06008-5
24. Yuan J, Tian J, Liu R, et al. Coactivator associated arginine methyltransferase 1 modulates cartilage degeneration and chondrocyte apoptosis in osteoarthritis by regulating ERK1/2 signaling pathway. *Aging Cell*. 2025;24(8):e70122. doi:10.1111/acel.70122
25. Xiang W, Zhang T, Li B, et al. Senescent macrophages induce ferroptosis in skeletal muscle and accelerate osteoarthritis-related muscle atrophy. *Nat Aging*. 2025;5(7):1295–1316. doi:10.1038/s43587-025-00907-0
26. Lee H, Lim J, Oh M, Lee J. Synergistic protective effects of oleaster fruit and Sophora japonica L. Fruit extracts against IL-1β-induced inflammation in human chondrocytes. *Foods*. 2025;14(17):3099. doi:10.3390/foods14173099
27. Yang H, Chen C, Chen H, et al. Navitoclax (ABT263) reduces inflammation and promotes chondrogenic phenotype by clearing senescent osteoarthritic chondrocytes in osteoarthritis. *Aging*. 2020;12(13):12750–12770. doi:10.18632/aging.103177
28. Brunet A, Goodell MA, Rando TA. Ageing and rejuvenation of tissue stem cells and their niches. *Nat Rev Mol Cell Biol*. 2023;24(1):45–62. doi:10.1038/s41580-022-00510-w
29. Gravallese EM, Pettit AR, Lee R, et al. Angiopoietin-1 is expressed in the synovium of patients with rheumatoid arthritis and is induced by tumour necrosis factor alpha. *Ann Rheum Dis*. 2003;62(2):100–107. doi:10.1136/ard.62.2.100
30. Eitner A, Sparing S, Kohler FC, et al. Osteoarthritis-induced metabolic alterations of human hip chondrocytes. *Biomedicines*. 2022;10(6):1349. doi:10.3390/biomedicines10061349
31. Janssen JN, Batschkus S, Schimmel S, Bode C, Schminke B, Miosge N. The influence of TGF-β3, EGF, and BGN on SOX9 and RUNX2 expression in human chondrogenic progenitor cells. *J Histochem Cytochem*. 2019;67(2):117–127. doi:10.1369/0022155418811645
32. Collins JA, Kim CJ, Coleman A, et al. Cartilage-specific Sirt6 deficiency represses IGF-1 and enhances osteoarthritis severity in mice. *Ann Rheum Dis*. 2023;82(11):1464–1473. doi:10.1136/ard-2023-224385
33. Ji Q, Zheng Y, Zhang G, et al. Single-cell RNA-seq analysis reveals the progression of human osteoarthritis. *Ann Rheum Dis*. 2019;78(1):100–110. doi:10.1136/annrheumdis-2017-212863
34. Zhang H, Zheng C, Chen W, et al. PP2 alleviates the progression of osteoarthritis by inhibiting Wnt/β-catenin and activating TGF-β/Smad signaling. *Int Immunopharmacol*. 2023;124(Pt B):110948. doi:10.1016/j.intimp.2023.110948
35. Farinelli L, Riccio M, Gigante A, De Francesco F. Pain management strategies in osteoarthritis. *Biomedicines*. 2024;12(4):805. doi:10.3390/biomedicines12040805
36. Zhang Y, Ma J, Bao X, Hu M, Wei X. The role of retinoic acid receptor-related orphan receptors in skeletal diseases. *Front Endocrinol*. 2023;14:1302736. doi:10.3389/fendo.2023.1302736
37. Wang G, An Y, Zhang X, Ding P, Bi H, Zhao Z. Chondrocyte spheroids laden in GelMA/HAMA hybrid hydrogel for tissue-engineered cartilage with enhanced proliferation, better phenotype maintenance, and natural morphological structure. *Gels*. 2021;7(4):247. doi:10.3390/gels7040247
38. Yu XJ, Zhao YT, Abudouaini H, et al. A novel spherical GelMA-HAMA hydrogel encapsulating APET×2 polypeptide and CFIm25-targeting sgRNA for immune microenvironment modulation and nucleus pulposus regeneration in intervertebral discs. *J Nanobiotechnology*. 2024;22(1):556. doi:10.1186/s12951-024-02783-z